Single Cells Can Resolve Graded Stimuli

Mirna Kramar,[1] Lauritz Hahn,[2] Aleksandra M. Walczak,[3,4,*] Thierry Mora,[3,†] and Mathieu Coppey[1,‡]
[1]*Institut Curie, Physics of Cells and Cancer, UMR 168, 75005 Paris, France*
[2]*Laboratoire de Physique de l'École Normale Supérieure, 75005 Paris, France*
[3]*Laboratoire de Physique de l'École Normale Supérieure, CNRS, PSL University, Sorbonne Université, and Université de Paris, 75005 Paris, France*
[4]*Applied Physics Research Group, Vrije Universiteit Brussel, Brussels, Belgium*

(Received 28 October 2024; accepted 27 October 2025; published 2 December 2025)

Cells use signaling pathways as windows into the environment to gather information, transduce it into their interior, and use it to drive behaviors. MAPK (ERK) is a highly conserved signaling pathway in eukaryotes, directing multiple fundamental cellular behaviors such as proliferation, migration, and differentiation, making it one of few central hubs in the signaling circuitry of cells. Despite this versatility of behaviors, population-level measurements have reported low information content (<1 bit) relayed through the ERK pathway, rendering the population barely able to distinguish the presence or absence of stimuli. Here, we contrast the information transmitted by a single cell and a population of cells. Using a combination of optogenetic experiments, data analysis based on information theory, and numerical simulations, we quantify the amount of information transduced from the receptor to ERK, from responses to singular, brief, and sparse input pulses. We show that single cells are indeed able to resolve between graded stimuli, yielding over 2 bits of information, however showing a large population heterogeneity.

DOI: 10.1103/pyf8-y4kt

I. INTRODUCTION

After decades of almost exclusive focus on behavior, learning, and decision-making in neural organisms, the attention is slowly shifting not only to non-neural organisms, but also the building blocks of all organisms: single cells [1]. Information processing is at the heart of these phenomena. Understanding how the information is taken up, relayed, and integrated is crucial to decoding the way decisions are made and behavior is executed on all levels of life.

In cells, information about the environment is relayed through signaling pathways. The signal taken up at the receptor is transduced through a complex network of proteins which act as biochemical modification cascades (e.g., by phosphorylation or conformational change), propagating the signal towards the nucleus for regulation of gene transcription, or to other hubs of the signaling circuitry, ultimately leading to behavioral decisions such as proliferation, migration, or apoptosis.

The existence of a range of cellular decisions resulting from a comparatively small number of signaling hubs inspired a number of studies aimed at elucidating cellular information processing strategies [2]. In particular, the bulk of these studies focused on the mitogen-activated protein kinase (MAPK) pathway, a signaling pathway implicated in key cellular functions. The most intensely studied subnetwork of the MAPK pathway—commonly referred to as the ERK signaling pathway—is a cascade of four kinases: Ras, Raf, MEK, and ERK [3].

A deep dive into the intricacies of ERK pathway signaling reveals a multitude of isoforms, mechanisms, and feedbacks [4,5]. One of the essential questions about information processing in a signaling cascade is its sensitivity to signals, which can be addressed from different perspectives—by asking questions about the nature of ligands, binding affinity, ligand dynamics, concentrations, and noise [6–9]. In the context of concentration, the ability to resolve between graded inputs can be quantified as the amount of information relayed when a stimulus is applied at different magnitudes. Traditionally, signaling pathways have been regarded as binary switches—active or inactive, devoid of the ability to resolve between different input states. Within the framework of information theory, the amount of information is estimated in bits: 1 bit for an on/off switch, and >1 bit for the ability to resolve graded inputs [10,11].

Studies addressing the information content in key signaling pathways reported a surprisingly small information content. A study of ERK and NFkB signaling pathways showed that the information capacity is less than 1 bit when considering a single feature of the response signal, such as the amplitude of the response, albeit around 1.5 bits when taking into account dynamical features of the response [12]. However, the input stimulus in the form of a diffusible ligand remains present after initial application, resulting in a continuous and adaptive response. Another recent study presented

*Contact author: aleksandra.walczak@ens.fr
†Contact author: thierry.mora@ens.fr
‡Contact author: mathieu.coppey@curie.fr

Published by the American Physical Society under the terms of the Creative Commons Attribution 4.0 International license. Further distribution of this work must maintain attribution to the author(s) and the published article's title, journal citation, and DOI.

a higher information content (2.3 bits), however it was attributed to multimodal perception (combinatorial encoding through several features including cell-intrinsic and environmental properties), stressing that noncontextual information content in the ERK pathway does not exceed 0.7 bits [13]. Effectively, this means that by relying solely on information transduced through the ERK pathway, cells are unable to distinguish between the presence and absence of stimuli, i.e., falling short of operating as an on/off switch.

Given the essential role of the ERK pathway in directing a range of core cellular functions, the reported low resolution between inputs is surprising and suggests that the question of the amount of information carried by the ERK pathway is still open [14]. Namely, the methods used in the listed studies present several challenges, which could have a significant impact on the measured information quantity. First, by averaging out the responses to the stimulus across the cell population, the individuality of the cells arising from the differences in their biochemical content is erased [15,16]. If the cell-to-cell variability in the response to stimuli (i.e., the extrinsic noise) is high, averaging the responses over the population could render the amount of information low for an average cell, regardless of a possible high information content in single cells [17,18]. Next, single-cell quantification within the information-theoretic framework requires building probability distributions, i.e., recording responses of single cells to various repeated stimuli. This is not reliably achievable with diffusible ligands due to the effects of ligand trapping, and a changing cell medium may impact cellular functions, introducing additional uncertainty [19]. Finally, relying on diffusible ligands allows only a small number of input states. Given that the maximum theoretical amount of information that can be transduced is given by the number of input states, having a range of well-resolved input states is essential [16]. A recent study reporting higher information content in the ERK pathway highlights the importance of single-cell measurements [20], however in the absence of single-cell data, it relies on theoretical modeling for quantification. An earlier experimental work suggested that the information content based solely on the amplitude of the response may exceed 1 bit when accounting for cell-to-cell variability [21].

Here, we revisit the question of information content in the ERK signaling pathway by introducing an experimental and quantification strategy to overcome the challenges faced by the studies presented above. We perform optogenetic stimulations of the MAPK pathway, carrying out an unprecedented number of repeated stimulations with seven light doses, and we quantify the mutual information in single cells using an algorithm specifically developed for application in cell signaling [22]. We find a large variation in the encoding features of single cells within the population, demonstrating the crucial importance of single-cell quantification. We show that some cells transmit over 2 bits of information, close to the maximal possible value set by the seven input stimuli (2.8 bits) which is significantly higher than previously reported for single pulses (i.e., nonsustained) of input. This result confirms our intuition about the cell's ability to noncontextually resolve graded inputs through the ERK pathway. Furthermore, to account for the limitations of our setup, we perform numerical simulations of optogenetic activation of ERK. The results of the simulations corroborate our experimental findings and highlight the importance of repeated stimulation. Finally, we look for patterns behind the intrinsic differences in information content in the population, and we discuss their implications in the functioning of the cell collective, as well as the generation of behavior.

II. RESULTS

A. Optogenetics allows for accurate estimation of mutual information in the ERK signaling pathway

There have been a number of constraints impeding the quantification of information flow in the ERK signaling pathway using the information-theoretic framework: the limited number of well-resolved inputs, the small number of samples due to an inability to perform repeated single-cell stimulation, limitations in the biosensor dynamic range, noise in the measurement, and nonoptimal distribution of stimuli with respect to the sensitivity of the pathway.

We tackle these constraints by building the experimental setup and the data analysis routine presented in Fig. 1. We mimic the varying input concentrations on the Fibroblast growth factor receptor (FGFR) by using its optogenetic analog, OptoFGFR1 [23] stably introduced in MCF10A cells, and we apply single short pulses of blue laser light of different strengths to activate the pathway. It was previously shown that this optogenetic molecular system responds gradually to light doses [25], and we optimize the light doses to span the whole dynamic range of cell responses [see Fig. S1 of the Supplemental Material (SM) [24]].

The kinase translocation reporter (KTR) is a fast-reacting and ERK1/2-specific fluorescent reporter [26] which reversibly shuttles out of the nucleus when ERK is activated [Fig. 1(a)]. Using a fluorescent histone label H2B-iRFP for nuclear segmentation, we quantify the ratio between cytosolic and nuclear KTR, thus obtaining a ratiometric readout of ERK activation robust to fluctuations in laser intensity and focus.

We carry out simultaneous stimulation of the ERK pathway in each cell in the population using seven light doses of increasing intensity, then we repeat the cycle 20 times. In the other main dataset, we repeat the stimulation cycle 15 times, and the light doses within each cycle are applied in this order: 1-7-3-6-4-5-2 (1 = weakest, 7 = highest). In each experiment, we use a gap of 30 min between each stimulus to allow for ERK deactivation, the total imaging time being 93.6 and 81.6 h, respectively. Additionally, in the main dataset (20 repeats), we measure the light intensity of each light dose with a power meter mounted above the imaging dish in the light path of the laser. This simultaneous recording of the light power allows for quantification of variability at the level of the input, estimated to be around 10–20% (Figs. S2 and S3 of the SM [24]).

Figure 1(b) shows the raw trajectories of ERK activation in individual cells over the course of the experiment. We obtained 20 cells across three different stage positions in the main dataset (20 repeats), and 40 cells in the other dataset (15 repeats) presented here. This apparently low number of cells is the result of selection criteria that arise from experimental limitations. The very long imaging times such as those in our experiments come with significant caveats: cells divide, migrate out of the field of view, and apoptose, all of which

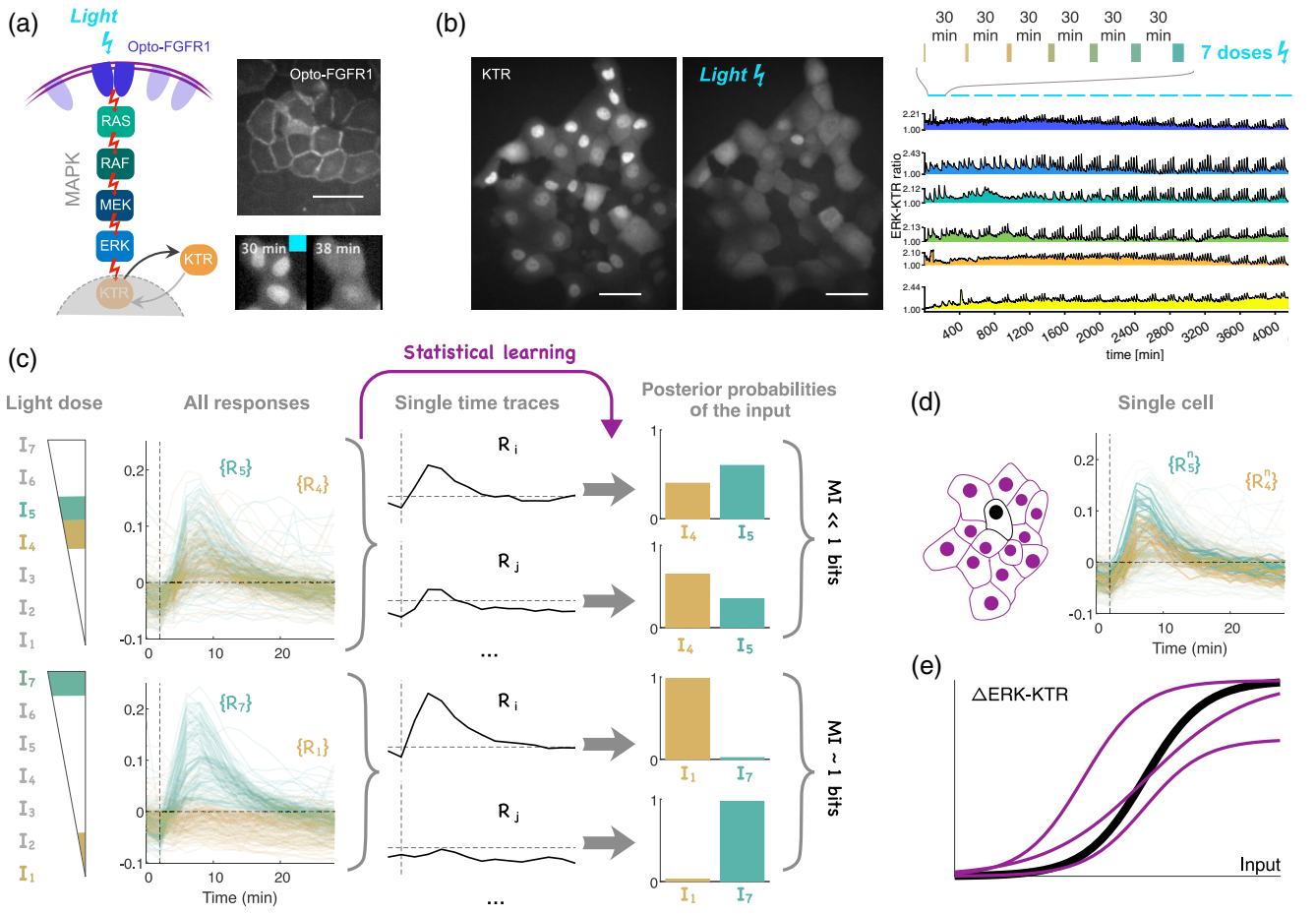


FIG. 1. Measuring mutual information of the MAPK pathway with many repeats at the single cell level. (a) Scheme of the MAPK signaling cascade activated by light. The optogenetic actuator OptoFGFR1 [23] consists of the fusion between truncated fibroblast growth factor receptor 1 (cytosolic domain, without the extracellular part) and CRY2, together with a fluorescent reporter (mCitrine). The construct localizes at the plasma membrane (top fluorescent image; scale bar is 100 μm), and when illuminated with blue light, CRY2 oligomerizes leading to the transphophorylation of the cytosolic tail of FGFR1 and thus receptor activation. Once activated, the receptor activates the MAP kinase phosphorylation cascade ending in the double phosphorylation of ERK, ppERK. We used ERK-KTR-mKate2 as a reporter of ERK activity, which is a minimal substrate domain that shuttles out of the nucleus when phosphorylated by ppERK (bottom fluorescent images, before activation and 8 min after; scale bar is 100 μm). (b) Round of optogenetic stimulations. Left: example of the whole field of view during the acquisition, before activation and 5 min after a light pulse (the full time series is available in the SM [24] as Video 1 and Video 2). Right: ridge plot depicting the ratios of cytosolic over nuclear ERK-KTR intensities for six example cells from one stage position, over the whole duration of the stimulation routine, which consists in 20 repetitions of 7 light pulses of increasing dose 30 min apart. The values in the plot are normalized by the smallest value of the ERK-KTR ratio for each ridge (i.e., trajectory). (c) Estimation of mutual information (MI). The seven light doses of increasing strength lead to a gradual increase of the cells' ERK responses. For two close light doses (here the fourth and the fifth light doses, I_4 and I_5), there is a strong overlap of the compiled cell responses [all selected cells and all repeats, shown in the top plot as $\{R_4\}$ (gold) and $\{R_5\}$ (turquoise)], whereas for the two extreme light doses (I_1 and I_7), cell responses appear distinguishable. In our pipeline, the statistical learning-based SLEMI algorithm [22] assigns posterior probabilities of the input stimulation. For clarity of presentation, here we only show the posterior probabilities of the input for two inputs. When cell responses have a large overlap, the posterior probabilities of the input are close to 0.5 (top, low mutual information), whereas when cell responses are distinguishable the probabilities are close to 1 (bottom, mutual information close to its maximum of 1 bit for two states). (d) Single cell responses are more reproducible than the whole population. When only one cell is selected among the field of view (black cell), even for two close stimuli the cell responses appear more distinguishable than the whole population (10 repeats for I_4 and I_5 stimuli of the best-performing cell are represented over all cells and repeat responses). (e) Each cell responds specifically. The differences of response overlap between all cells and the selected cell can be explained by the fact that every cell has its own perception of stimuli. Here, the dose-response curve of neighboring (purple) cells could diverge from the selected (black) cell by a shift in the half-maximum, a change of sensitivity (slope), or dynamic range (amplitude).

can render their signal noncontinuous or unreliable for further quantification. Equally, cells with an insufficient amount of visible cytoplasm around the nucleus (e.g., when squished between neighboring cells during migration) do not allow a quantification of cytoplasmic KTR. Equally, fluorescent debris from dead cells floating over the imaged population presents challenges for signal extraction. For these reasons, only cells that display a reliable, continuous signal and stable

morphology over the whole course of the experiment were considered. Cells that do not show a response to some of the stimulation cycles, but present a reliable signal, are nonetheless kept for further analysis.

It is also worthwhile to note that the cells are imaged in the presence of serum, which is an important distinction from the usual protocol for imaging ERK activity used in existing studies. Although the presence of the serum enhances basal ERK activity [27], it is necessary for cell survival on the timescale of days, and it supports physiological conditions, which is desirable when discussing the results in the context of organismal function.

The quantification pipeline is presented in Fig. 1(c) and detailed in Appendix B. The time series of single-cell ERK activity over the duration of the whole experiment are detrended by a moving averaging window and subsequently fragmented into 30 min trajectories, starting with the application of the stimulus and ending one timepoint before the application of the next stimulus. To account for the fact that cell responses are time-varying signals that may contain information beyond a single given timepoint, we extracted a vector containing the values of the response over a temporal window. Likewise, we also applied a dimensionality reduction method [principal component analysis (PCA)] to compress the whole response trajectories into a few components.

Next, we used these features (vector-containing ERK responses and principal components) as input in the Statistical Learning Estimator of Mutual Information (SLEMI) [22], which we found to be best-performing among several mutual information estimators we tested according to different criteria (see Appendix A and Fig. S4 of the SM [24]). The algorithm estimates information-theoretic quantities between a finite state input and a continuous output using logistic regression [22].

For each input condition x_i, $i = 1, \ldots, N$, the experiment is repeated to obtain n_i samples y_i^j, $j = 1, \ldots, n_i$. SLEMI uses multinomial logistic regression to infer the distribution $P(x_i|y_i^j)$ from the data, such that the MI can be approximated as

$$I(X;Y) \approx \sum_{i=1}^{N} \frac{P(x_i)}{n_i} \sum_{j=1}^{n_i} \log_2 \left(\frac{P(x_i|y_i^j)}{P(x_i)} \right). \tag{1}$$

The importance of performing the analysis on single-cell data is outlined in Figs. 1(d) and 1(e). The varying biomolecular makeup of each cell necessitates single-cell analysis since the individuality of each given cell may distort their perceptions of stimulus intensity. For the estimation of mutual information, this implies that only repeated measurements of the response of a single cell will overcome the extrinsic variability, which manifests as a lack of reproducibility at the population level.

B. Population-level readout erases the input resolution abilities of single cells

We quantify the mutual information (MI) between the values of the light doses (input) and the time trajectories of the cytoplasmic-to-nuclear ratio of ERK-KTR fluorescence (output). The results of the quantification are depicted in Fig. 2. These temporal trajectories were compressed by selecting timepoints or by PCA, as described in the preceding section. In the first case, we initially only consider the first timepoint after stimulation, then successively calculate the MI using trajectories over time windows of increasing length. In the second case, we start with only the first PCA component and then add further components in order of decreasing variance. We also quantified the MI using the area under the trajectories, which could be easily extracted by a downstream transcriptional network through simple integration of the signal (Fig. S5 of the SM [24]).

Given that we used seven light doses, the maximum MI is set by $\log_2(7) \approx 2.8$ bits. When considering individual cells, the population average of the mutual information reaches a plateau around 1.5 bits when four timepoints or four principal components (or more) are taken. However, when all cell responses are pooled, the maximal information content drops to $\approx$0.5 bits, a low value showing that the pooled responses of the cells are strongly overlapping and preventing the stimuli from being distinguished. This mutual information can be slightly increased to $\approx$0.7 bits considering only the lowest and highest stimuli (Fig. S6 of the SM [24]), with the population still unable to clearly distinguish between the presence and absence of stimuli.

The higher mutual information in single cells compared to the population experimentally confirms the crucial importance of single-cell analysis, and it shows that single cells are able to resolve between several intensities of the stimulus. Furthermore, the results reveal a large variability in information content within the population (Fig. 2), with some cell responses yielding over 2 bits of information, the highest being 2.2 bits. Such a large value shows that cells can almost reach the maximal theoretical mutual information.

Finally, we probe the relationship between the information content and the expression level of the optogenetic receptor. We calculate the pooled information for low- and high-expressing subpopulations of cells, and we find that overall high levels of OptoFGFR lower the mutual information. This surprising result appears to be caused by an intrinsically increased variability over time in OptoFGFR expression in these cells, which then likely decreases the reproducibility of cell responses between stimulation repeats (Fig. S7 of the SM [24]).

C. Information is contained in response dynamics

We next investigate the informative abilities of individual timepoints in the cell responses, as well as in individual principal components obtained by dimensionality reduction (PCA). We find that the third and fourth timepoint are the most informative with around 1 bit of information (Fig. 2). The same amount of information is obtained from the first PCA component. The third and fourth timepoints are closest to the peak of the response trajectories, making it the most informative feature of the response. By reading out just the response peak, single cells can on average distinguish between the presence and absence of the stimulus. When considering pooled cell responses, the information content of single timepoints follows a similar trend to that of single-cell responses, but without the ability to discriminate between stimuli.

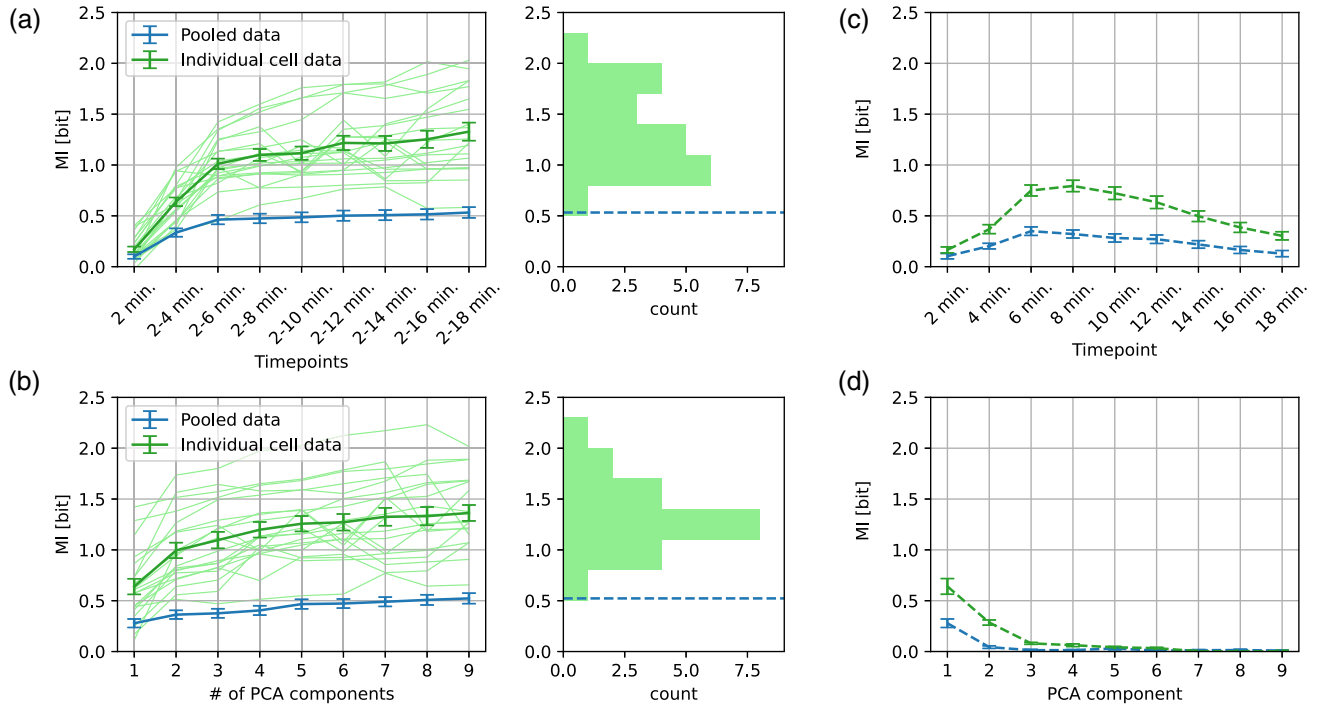


FIG. 2. Population-level readout erases the input resolution abilities of single cells. (a) Mutual information contained in single cells vs the population. Mutual information calculated by taking single-cell trajectories (light green) and by pooling the trajectories and thereby erasing the cell identities (blue) shown for an increasing number of timepoints, sampled every 2 min. The average information quantity contained in single-cell trajectories is shown in dark green. The histogram depicts the distribution of the mutual information extracted from the last data point of single-cell trajectories (green), with the dashed blue line marking the mutual information value for pooled trajectories. (b) Analogously, quantification of mutual information for an increasing number of principal components (sorted by variance) of response trajectories, and the corresponding histogram of mutual information values. (c) Mutual information from single-cell trajectories contained in individual timepoints (given in minutes after light stimulus) for the average of the single-cell data (green) and pooled trajectories (blue). (d) Analogously, the mutual information contained in individual principal components for single-cell trajectories (green) and pooled trajectories (blue).

D. Cell-to-cell variability in responses is large but appears to be unrelated to endogenous ERK fluctuations

Having observed large differences in information content, we delve deeper into cell-to-cell variability to understand how information content degrades when pooling cell responses. We first introduce a signal decoder to compare the true input with the input that is predicted by the cell. The predicted input is the dose with the highest assigned probability in the multinomial logistic regression performed in the SLEMI algorithm, averaged over the different repeats of the stimulus. Thus, the predicted dose index for input dose i is given by $(1/n_i)\sum_j \mathrm{argmax}_k P(x_k|y_i^j)$, with n_i and $P(x_k|y_i^j)$ as described above.

Using the decoder based on the pooled cell model, we compare the decoding abilities of individual cells belonging to a population at one stage position, i.e., cells that received the same input doses. These results are presented in Fig. 3(a), where unbiased decoding is depicted by a dotted black line across the diagonal. While none of the cells display unbiased decoding using the pooled cell model, some cells perform close to population average, while other cells strongly diverge from it. The changing slope for individual cells reveals an interesting feature: the cells' decoding behavior changes with the light doses. This behavior is unlikely to be time-dependent since the cell model is calculated from repeats occurring periodically over the course of the whole experiment (days), and more likely informs about a cell's sensitivity to a dose range with respect to the population. The need for individual (single-cell) decoders is shown in Fig. 3(b), where all cells perform close to unbiased decoding of the input signal (dotted black line).

Next, we focus on the potential role of endogenous fluctuations in ERK activity in response to stimuli and information encoding. High endogenous fluctuations, coming from either spontaneous activities or cell-to-cell communication, may sum up with the optogenetic activation and deteriorate the amount of information being transduced. In Fig. 3(c), we compare the magnitude of endogenous ERK activity fluctuations during the imaging phase without stimulation to the magnitude of ERK response to light stimuli. As an example, we compare three cells, two of which show the highest deviation in their decoding ability from the prediction using the pooled cell model in Fig. 3(a), and one of them performs close to perfect decoding using the pooled cell model. The cell with high endogenous fluctuations (in purple) shows a high ERK response magnitude, and the cell with low endogenous fluctuations (in orange) displays comparatively low ERK response magnitude, hinting that the endogenous ERK activity could alter the response to stimuli. However, the third (green) cell displays a comparably high ERK response magnitude and low

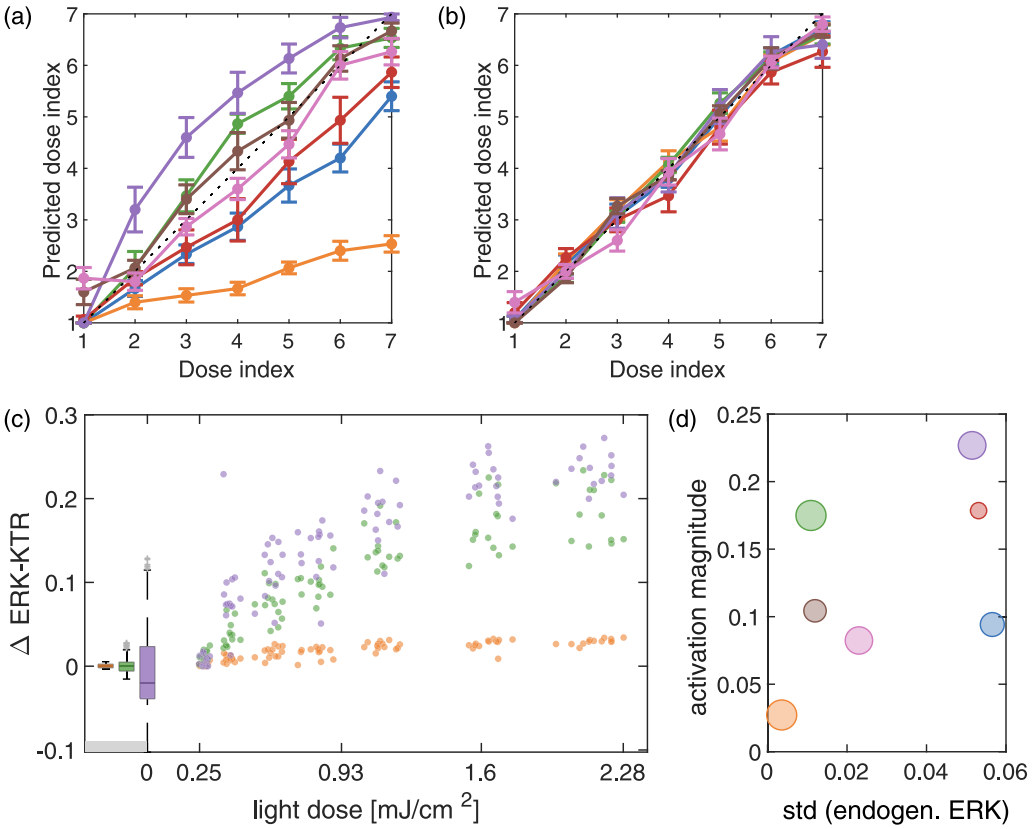


FIG. 3. Large intrinsic variability demonstrates the need for individual decoders. (a), (b) Light dose inferred by the cell against the actual light dose using the pooled cell model decoder (a) and individual cell model decoder (b), calculated for all cells in one stage position. Unbiased decoding is shown as a dotted black line. (c) The relationship between the endogenous fluctuations in ERK activity and the responses to light stimuli for three cells from the previous panels (a), (b): two of the cells deviate most strongly from the pooled cell model prediction (orange and purple), and one performs close to perfect decoding when using the pooled cell model (green). The box plot on the bottom left depicts the range of endogenous fluctuations of ERK activity for each of the cells (i.e., in the absence of light stimuli, marked by a gray bar). The response of the cells to the light stimuli is shown as a scatter plot for each of the three cells, where Δ ERK-KTR is the difference between the ERK-KTR ratio for the given light dose and the ERK-KTR ratio for the weakest dose. (d) Using the same color code, the maximal response magnitude of the cells, i.e., the difference between ΔERK-KTR for the highest and lowest light dose, is shown against the standard deviation of the endogenous fluctuations. The mutual information content for each cell is depicted by the size of the marker. The association between the mutual information measured in cells, the magnitude of ERK activation, and the magnitude of endogenous fluctuations was tested using Spearman's Rank Correlation and Kendall's Tau test, which did not report a statistically significant correlation.

endogenous fluctuations. The plot containing all cells can be found in Fig. S8 of the SM [24].

To further delve into this question, we compare the mutual information of each of the seven cells while simultaneously depicting the maximum ERK response to stimuli against the standard deviation of endogenous ERK fluctuations [Fig. 3(d)]. Due to the small sample size, we use both Spearman's Rank Correlation and Kendall's Tau test to assess the relationships between these three variables. First, we find a weak positive correlation between endogenous fluctuations and maximum ERK response, however not statistically significant in either test (Spearman's $\rho = 0.393$, $p = 0.396$; Kendall's $\tau = 0.238$, $p = 0.562$). Next, endogenous fluctuations and mutual information show a moderate negative correlation (Spearman's $\rho = -0.643$, $p = 0.139$; Kendall's $\tau = -0.429$, $p = 0.239$), suggesting that higher endogenous fluctuations could be associated with lower mutual information. However, this association was not statistically significant, although it did approach significance in Spearman's test. Finally, the correlation between response to stimuli and mutual information is very weak and negative, and not statistically significant in either test (Spearman's $\rho = -0.179$, $p = 0.713$; Kendall's $\tau = -0.238$, $p = 0.562$).

Given the absence of convincing evidence of association, the endogenous ERK activity did not prove to be a driving factor causing cell-to-cell variability, and optogenetic stimulations might overcome these spontaneous activities irrespective of their strengths. Taken together, we conclude that the main driver of cell-to-cell variability is a variable encoding scheme that is specific for each cell, i.e., the ability to distinguish between different stimuli is specific to each cell and independent of the lineage or the local environment, most likely stemming from the difference in their intrinsic molecular makeup.

E. Numerical model corroborates experimental results and bridges scales

Having a sufficient number of samples is a known challenge for accurate estimation of information within the information-theoretic framework [28,29]. Even with the unprecedented number (20) of samples, i.e., repeated stimulation of single cells that we present here, inferring the reliability of the information estimate remains a challenge in this complex biological system. To this end, we use a published kinetic model of the ERK pathway (Fig. S9 of the SM [24]) with parameters sampled from experimental data [25], and we perform numerical simulations of optogenetic activation of the pathway with light doses mimicking the experimental ones (Fig. S10 of the SM [24]). We create a set of 400 virtual cells by generating random combinations of parameters, allowing a variation of up to 18% for each parameter to account for cell-to-cell variability, and we perform 1000 repeats of stimulation with each light dose. The resulting simulation trajectories are further modified by adding 1% Gaussian white noise to each time point of the simulated trajectories to avoid having overly similar trajectories during the inference.

Then, we subject the obtained response trajectories to the same analysis pipeline as used for the experimental data. Figure 4(a) depicts the information contained in the time traces using the two feature reduction techniques already described above. The results of the simulations agree with the experimental findings: the information contained in single-cell responses greatly surpasses that contained in pooled data. The average single cell in the simulations performs better than its experimental counterpart likely due to a lesser degree of additive noise, which in the experiments arises from various sources: biological, experimental, and postprocessing. The mutual information contained both in the pooled and single-cell trajectories rapidly increases when the noise added to the trajectories is decreased (Fig. S11 of the SM [24]); however, it is important to note that even with very low noise, the information content in best-performing simulated cells barely exceeds 2.5 bits. This information content, smaller than the theoretical maximum (2.8 bits), indicates the upper bound due to the variability of the input.

The satisfying degree of resemblance between the simulated and experimental cells now allows for probing the role of the number of stimulation repeats on the estimate of mutual information [Fig. 4(b)]. Both timepoint-based trajectories and PCA components used as input result in strong fluctuations in MI value for small sample sizes. After approximately 100 repeats, the curve stabilizes around a lower value of about 1.9 bits. The initial fluctuations of the MI value indicate that the number of repeats in our experiment (marked with a dashed line) is the minimum required for a reliable estimate, being at the start of a monotonic behavior of the curve. This result shows that the experimental values of mutual information should be taken with some caution: simulations show that we might be overestimating the mutual information for our experimental sample size, however only by about 10%. In the case of low noise levels, the MI reaches a stable value of about 2.5 bits already for 20 samples (Fig. S11 of the SM [24]). These results further emphasize the role of noise in the estimation of mutual information. Furthermore, to test the effect of

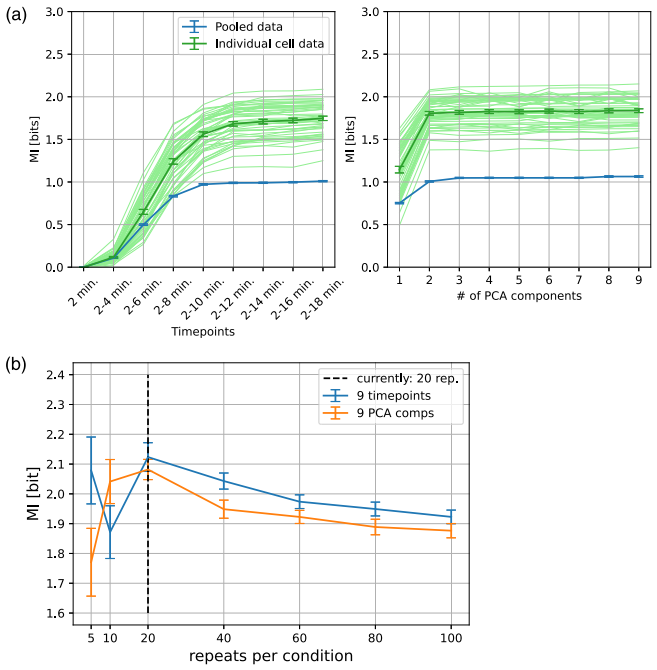


FIG. 4. Numerical simulations corroborate experimental findings. (a) Simulations of optogenetic activation of the MAPK cascade, akin to the experiments. Analogously to Fig. 2, mutual information contained in the simulated cells' ERK response trajectories was calculated using an increasing number of timepoints (left) and PCA (right). The results from pooled cell responses are shown in blue, and the results from single-cell responses are shown in green (individual cells are in light green, the average of single-cell responses are in dark green). For clarity of presentation, a subset of 40 simulated cells was selected for this visualization. (b) The estimation of mutual information in simulated trajectories here for a different number of repeats per condition. The information is estimated using the first nine timepoints (blue) and nine PCA components (orange). The value of mutual information undergoes fluctuations for a low number of repeats, and stabilizes after $\approx$ 100 repeats. The black dashed line is drawn at 20 repeats per condition, the current experimental limit.

the number of cells in the estimate of the mutual information, we perform a bootstrapping calculation on the experimental and simulation results, and we find that the sample size in our experiments is sufficient for a reliable MI estimate (Fig. S12 of the SM [24]).

The numerical model also enables direct evaluation of how specific kinetic steps shape the system's ability to transmit information. While we do not compute mutual information for each parameter variation, we quantify how changes in parameter values alter the distinctness of ERK response trajectories across input conditions, which is a prerequisite for high mutual information. The analysis with different metrics consistently identifies a core set of regulatory steps that dominate system sensitivity (Fig. S13 of the SM [24]). These include the phosphorylation and dephosphorylation of the KTR reporter by ERK, which control how ERK activity is encoded in the observable output; the Ras-Raf signaling module, which integrates upstream signals and is subject to feedback; and the ERK-driven negative feedback loop that modulates Raf activity and enforces adaptive dynamics. Additional

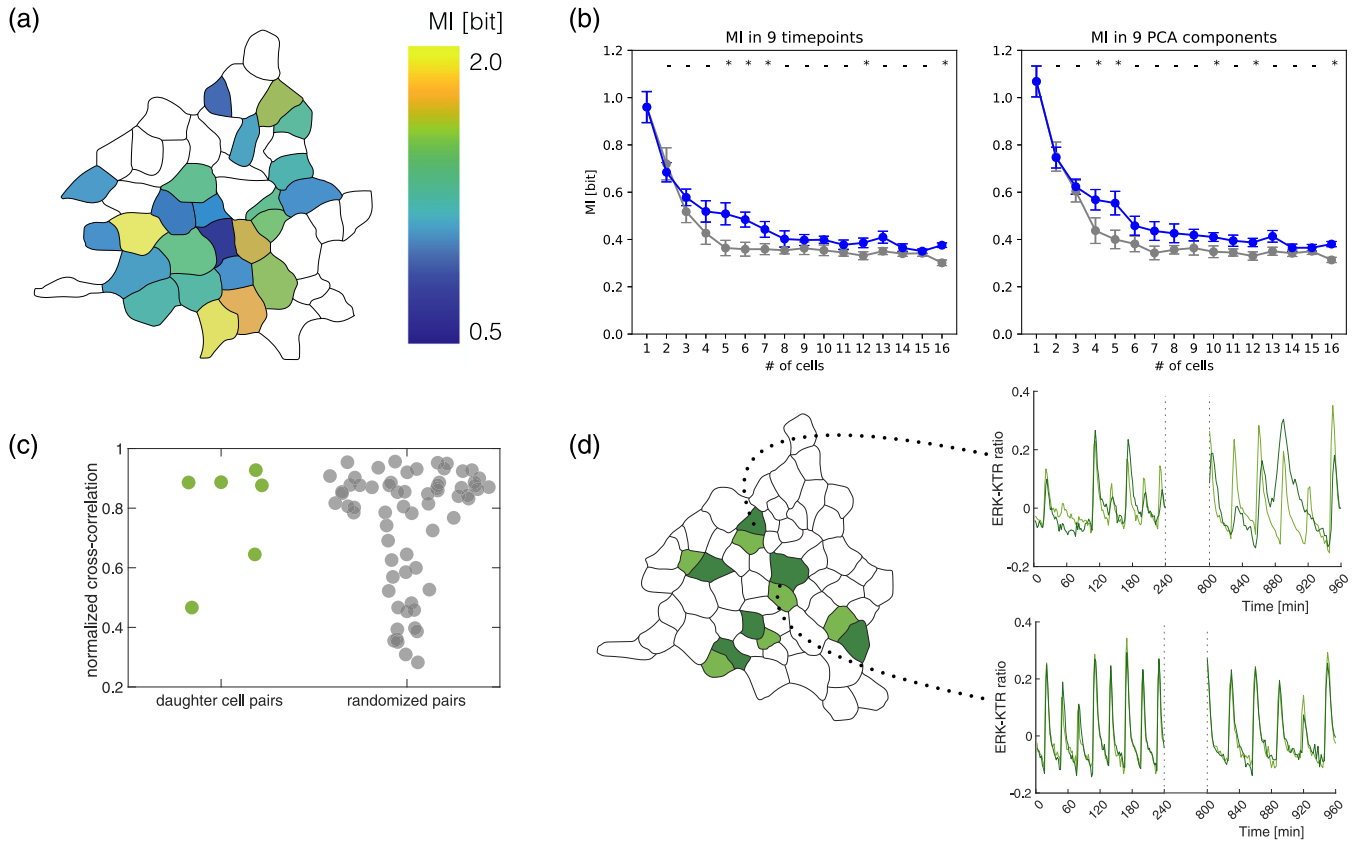


FIG. 5. Spatiotemporal aspects of mutual information in the cell collective. (a) Spatial distribution of mutual information in a cell population, obtained from nine timepoints of the response trajectories (left). Only the cells that passed selection criteria for analysis are taken into account, otherwise shown in white. (b) Mutual information (from nine timepoints and PCA nine components, as described above) calculated for clusters of neighboring cells of different sizes (number of cells in a cluster on the x axis) compared to the mutual information in clusters of the same size, but with cells drawn from random positions in the population. The curves depicting the information in clusters of actual neighbors fall off slightly slower compared to the randomized clusters. Top of the plot: Mann-Whitney U test, with (–) and (*) indicating a p-value above and below 0.05, respectively. (c) Comparison of the values of cross-correlation of ERK response signal between two daughter cells to randomized pairs shows no indication of increased correlation in the pair. Tested by a Kolmogorov-Smirnov test, $p = 0.3744$. (d) Example ERK response trajectories for the marked daughter cell pairs, where two extreme cases are shown: uncorrelated cell responses (top) and highly correlated ones (bottom).

sensitivity arises from the receptor activation of Ras and from the phosphorylation cycles within the MAPK core that govern amplification and timing.

These nodes represent the system's main kinetic bottlenecks. They define where input distinctions are preserved or lost, and where tuning alters the dynamic range and resolution of input states. This mapping establishes how the architecture of the pathway constrains its information-processing capacity.

F. Spatiotemporal aspects of information in a cell collective

We further address the question of cell-to-cell variability by examining potential spatial patterns of information in a cell collective. The experimental findings presented above show that mutual information drops strongly from one cell to the whole population [Fig. 2(a)]. Here, two scenarios can be envisaged. First, neighboring cells could present a higher degree of similarity, either because they originated from the same cell, or due to their spatial proximity, whereby in both cases the mutual information would slowly decay when considering increasing groups of close-by cells. Alternatively, cells may have different identities, irrespective of their spatial distribution within the population, and mutual information would drop as the group of cells increases due to their variability in encoding inputs. To address this question, we use the other dataset (15 repeats) containing a higher number of cells per stage position, which passed the set criteria for analysis and also form a large patch of cells. Figure 5(a) depicts the spatial distribution of mutual information in the population of cells, with no obvious spatial pattern. A comparison of the mutual information in a patch containing a different number of neighboring cells with the information in a randomized patch shows that mutual information presents a slight spatial component that can be observed for groups of four to seven cells. However, neither smaller nor bigger groups present any statistically significant increase in mutual information compared to randomized groups, indicating a lack of a convincing spatial pattern.

To further test if two neighboring cells are as variable as the whole population, we focused on the most extreme case of anticipated similarity: daughter cells, i.e., two cells resulting from the same division event. Over the course of the experiment, six division events took place in this cell population.

Since they appear at different times and therefore do not satisfy the selection criteria for MI quantification, we cannot estimate the mutual information for these cells. However, we can examine the similarity of daughter cells' responses to light stimuli, and hence address the question of cell-to-cell variability. Figure 5(b) depicts the results of cross-correlation of the ERK response signal for pairs or daughter cells and randomized pairs. We used matlab built in a two-sample Kolmogorov-Smirnov test with the null hypothesis stating that both samples come from the same distribution. The test failed to reject the null hypothesis at the 5% significance level ($p = 0.3744$), meaning that in line with our previous observation, there is no significant difference in correlation between the two groups. This result indicates that daughter cells are as variable as two cells randomly picked from the population.

III. DISCUSSION

In this work, we addressed the question of information content in the ERK signaling pathway, with the specific aim of clearing the long-standing conundrum in the field that arose from experimental obstacles. We designed an experimental setup to carry out repeated optogenetic stimulations of single cells with inputs of seven different strengths, resulting in a large number of response trajectories. We evaluated the trajectories for information content using the information theory formalism, and we obtained mutual information measured in bits.

The experimental results show that pooling the ERK response trajectories from all cells results in a large loss of information, which renders the population barely able to distinguish between the presence and absence of stimuli, while single-cell response trajectories contain over 1.5 bits of information on average, with a fraction of cells yielding over 2 bits of information, i.e., effectively being able to distinguish between more than four input states. This result showcases the crucial importance of single-cell analysis, and it explains the apparent low information content reported previously.

Our numerical simulations of the optogenetic ERK pathway activation support the experimental results, as well as providing intuition about the accuracy of the mutual information estimate for a varying number of samples. We believe that our estimation of the mutual information can be taken as a lower bound given the experimental limitations. The measurements are bounded by experimental noise, including the biosensor dynamics, image acquisition, and data analysis routines, which are always imperfect, as well as the variability of the input itself (here 10–20%), and of course of the number of different stimuli.

Another possible factor contributing to noise is the slowly evolving trend in ERK responses (Fig. S14 of the SM [24]). Since the imaging takes over 4 days, the cells may drift in their own encoding scheme. Some cells display a monotonous drift over time (Fig. S15 of the SM [24]). Thus, the mutual information might be higher if the estimation could be performed on a shorter time window.

We delved deeper to identify the sources of the observed cell-to-cell variability, finding no evidence of the variability being linked to endogenous ERK fluctuations, and no convincing indication of a spatial pattern. Interestingly, we found that the variability from cell to cell was due to the differences in their encoding schemes, i.e., the cell-specific dose-response curves. This cellular specificity seems not to be inherited, since the responses of daughter cells were not more correlated than randomized pairs. It could be hypothesized that cells are equipped with adaptation mechanisms to either maintain their sensitivity set-point, or to filter out this extrinsic variability in the downstream integration [30,31] of ERK signals.

Our results agree with the previous findings of information being contained in response dynamics [12], which shows that single signaling pathways can encode more than an on/off state. As introduced earlier, cells can also distribute information through a combinatorial activation of several pathways [13]. We would like to stress here that the two mechanisms are not mutually exclusive, and an increase of information in a given pathway will further enhance the ability of cells to encode more subtle cues at the level of the whole signaling circuitry.

It is surprising that the magnitude of endogenous fluctuations of ERK activity does not seem to have a bearing on the cell's ability to encode information. In our experiment, the cells are imaged in physiological conditions, in the presence of serum, which normally activates the ERK pathway thanks to the presence of a variety of growth factors. However, we think that endogenous ERK fluctuations should not be hastily dismissed. Intriguingly, in the absence of optogenetic stimulation, we observed significant endogenous fluctuations on the same scale as the responses to the first two weakest inputs. Yet, those weak optogenetic inputs were eliciting reproducible and distinguishable cellular responses. Thus, cells may have a fast adaptation mechanism that allows signaling events to "shortcut" other ones. Alternatively, the repeated stimulation routine may have entrained the cells to lower their basal activity on a relatively long timescale ($\approx$1 h). It is interesting to notice that spontaneous ERK activity is happening in the lower range of response dynamics. In the context of our information-centered approach, it seems that cells do not exploit their full information capacity, or that we are underestimating the amount of mutual information in the lower range of inputs. It would be interesting for future studies to quantitatively assess the prior distribution of inputs in the generation of behavior, for example during development [26].

The observed endogenous fluctuations may also reflect cell-to-cell communication, since a cell's ERK activity is communicated to the neighbors [27]. However, the absence of correlation between daughter cells' ERK responses and the absence of clear spatial patterns suggest that cells respond to our stimuli in an autonomous fashion. This differs from scenarios where multicellular communication enhances sensitivity to weak stimuli, such as epithelial collectives detecting shallow EGF gradients beyond the capability of individual cells [32]. The direct experimental assessment of the role of cell-to-cell communication would require the use of isolated cells, but unfortunately, due to the very long duration of the experiment and the tendency of the cell line to grow in clusters, recording ERK responses to repeated stimuli on isolated cells is not achievable.

The nature of the input is another important aspect to consider when quantifying information in signaling pathways. A number of recent studies demonstrated the key role of input

dynamics on cellular behavior [33–36], and it is likely that temporally modulated signals may encode more information or higher specificity in cell response. It will be paramount for future studies to assess the quantitative aspects of the inputs in physiological conditions—whether the most significant part of the input comes from neighboring cells or from the ever-changing broader environment.

Likewise, in the pioneering study on the topic of information in signaling pathways [12], the input (ligand concentration) was sustained throughout the measurement, possibly allowing a reinforcement of the response and resulting in a high information content on the population level. In contrast, our study examined the response of the cells to very short pulses, spaced out in time to allow the return of ERK activity to its basal level. This important distinction accounts for a different biological scenario, where cells experience sparse pulses of stimulation. For example, spatial ERK activation waves triggered as a single pulse by an apoptotic cell coordinate the fate decision signaling in the epithelium [35]. The surprising variability in information content within the population invites questions about the heterogeneity in sensitivity to inputs, and its implications on subsequent cellular decision-making.

Overall, with the introduction of repeated stimulation and single-cell level quantification, this work removed a previously daunting obstacle to understanding cellular information processing, and it opened a way to study the link between information encoding and organization of behavior in populations of cells.

ACKNOWLEDGMENTS

This project has received funding from the European Union's Horizon 2020 research and innovation programme under the Marie Skłodowska–Curie Grant Agreement No. 101031499. The experimental setups and infrastructure used were supported by the LabEx Cell(n)Scale (ANR-10-LABX-0038), Labex and Equipex IPGG (ANR-10-NANO0207), Idex Paris Science et Lettres (ANR-10-IDEX-0001-02 PSL), French National Research Infrastructure France-BioImaging (ANR-10-INBS-04), and Institut Convergences Q-life (ANR-17-CONV-0005). We kindly thank Carine Vias for the preparation of plasmids for lentiviral transduction, Olivier Pertz for the MCF10A cell line and discussions, as well as Jan Mikelson and Mustafa Khammash for sharing their model and parameters of the MAPK pathway.

DATA AVAILABILITY

The data that support the findings of this article are openly available [37]; embargo periods may apply.

APPENDIX A: MUTUAL INFORMATION ESTIMATION

Several algorithms exist in the literature to estimate the mutual information between random variables, for example k-nearest-neighbor-based (knn) methods [12,38], Markov model-based methods [39], and methods using Bayesian inference [22]. We have tested and benchmarked several of these algorithms (Fig. S4 of the SM [24]), and found that the Bayesian inference-based SLEMI [22] algorithm performed best with our data.

For an input X taking N different, discrete values x_i and the continuous, time-dependent output $Y(t)$, the mutual information between X and $Y(t)$, in bits, reads

$$I(X;Y) = \sum_{i=1}^{N} P(x_i) \int \mathcal{D}[y(t)] P(y(t)|x_i) \log_2 \left(\frac{P(x_i|y(t))}{P(x_i)} \right), \tag{A1}$$

where $\int \mathcal{D}[y(t)]$ is a path integral over all possible trajectories $y(t)$. When repeating the experiment for a given input x_i a total of n_i times, the distribution $P(y(t)|x_i)$ is sampled. The SLEMI algorithm [22] uses the law of large numbers to approximate the MI as

$$I(X;Y) \approx \sum_{i=1}^{N} \frac{P(x_i)}{n_i} \sum_{j=1}^{n_i} \log_2 \left(\frac{P\left(x_i|y_i^j\right)}{P(x_i)} \right), \tag{A2}$$

where y_i^j, $j = 1, \ldots, n_i$ are the experimentally sampled trajectories. SLEMI then uses statistical learning to infer $P(x_i|y_i^j)$ from the data. Following the authors of that work, we use multinomial logistic regression for the inference step.

The other algorithms mentioned above estimate $P(y_i^j|x_i)$ to compute mutual information. However, this is a high-dimensional distribution and is generally difficult to estimate, so in general, SLEMI requires fewer samples per input condition to converge. In our experiments, only a very limited number of samples can be obtained from each cell ($\sim$20 per cell), so SLEMI's faster convergence is a significant advantage. Furthermore, SLEMI is a parameter-free estimator: unlike knn estimators, where an arbitrary value of k must be fixed, SLEMI does not contain any numerical parameters that need to be fixed.

Finally, the available knn-based estimators each have disadvantages relevant to the problem at hand. In particular, the original estimator by Kraskov, Stögbauer, and Grassberger [38] does not use discrete, but rather continuous variables as inputs, and we previously found that the algorithm by Selimkhanov *et al.* [12] struggles with high-dimensional outputs [40].

Nonetheless, care must be taken to avoid overfitting. When using seven different input conditions and a nine-dimensional output (nine timepoints or PCA components), $(7-1)\times 9 = 54$ parameters need to be fitted. To avoid overfitting, we found it necessary to add fivefold cross-validation and an L1 regularization penalty, to which end we reimplemented SLEMI in Python. Since the L1 norm is not invariant under linear transformations, we expect slight variations in the model depending on the parametrization of the data.

APPENDIX B: MATERIALS AND METHODS

1. Cell culture

The MCF10A breast epithelium cell line stably expressing the OptoFGFR-mCitrine was kindly gifted by the laboratory of Olivier Pertz (Universität Bern, Institute of Cell Biology). Subsequently, lentiviral transduction was used to generate a stable cell line expressing the H2B-iRFP histone marker, and the ERK-KTR-mKate2 reporter of nuclear ERK activity. The

cells were cultured in plastic-bottom cell culture flasks and a standard MCF10A medium. The medium contains 500 mL DMEM F-12 (Sigma), GlutaMAX (1%, Gibco), Horse serum (5%, Sigma), Human EGF (20 ng/mL, Sigma), Human insulin (0.1%, Sigma), Cholera toxin (100 ng/mL, Sigma), Hydroxycortisone (0.5 mg/mL, Sigma), and Penicillin-Streptomycin (1%, ThermoFisher Scientific).

2. Imaging setup

The imaging was performed on an epifluorescence imaging setup, composed of an Olympus IX83 inverted microscope, an electron-multiplying Evolve EMCCD camera (Photometrics), and a laser bench (Gataca Systems, Massy, France) equipped with the following lasers used here: 491 nm (activation of OptoFGFR1), 560 nm (excitaton of ERK-KTR-mKate2 reporter), and 640 nm (excitation of the H2B nuclear marker). The cells were imaged using a 20× Olympus air objective (NA 0.7).

The atmosphere in the stage top incubator is controlled by the CO2-Controller 2000 (Pecon) and the temperature controller TempControl 37-2 digital (Pecon). The laser illumination is controlled by the iLas2 software (Gataca Systems, Massy, France), and the imaging setup is executed using Metamorph software (Molecular Devices, Eugene, OR), through a custom-made Matlab script.

The light power of each light dose used for OptoFGF stimulation was measured with a ThorLabs PM100D power meter, and the measurement was executed automatically by a custom-made Matlab script. The sensor of the power meter was fixed to the glass cover of the stage-top incubator and protected from ambient light.

3. Live cell imaging and optogenetic activation

The cells were plated 24−36 h before the experiment on a 35-mm glass-bottom FluoroDish (Thermo Fisher), 120 000 cells per dish in a 2 mL FluoroBrite DMEM (Thermo Fisher) medium with 5% Horse Serum (Sigma), 1% GlutaMAX (Gibco), and 1% Penicillin-Streptomycin (Sigma). The addition of serum ensures cell viability and normal physiology over the multiday course of the experiment.

The acquisition was carried out every 2 min, and images were acquired in two channels. Images of the H2B-iRFP nuclear marker were acquired by 640 nm laser excitation for 200 ms, and the images of the ERK-KTR-mKate2 reporter were acquired by 640 nm laser excitation for 200 ms.

The excitation of the OptoFGFR optogenetic actuator with the 488 laser was performed every 30 min during the stimulation phase, starting 120 min from the start of imaging for the main dataset with 20 repeats, and 100 min for the other dataset with 15 repeats. After all the stimulation repeats are carried out, the imaging is continued for several hours. The phase without stimulation at the beginning and the end of imaging serves two purposes: to estimate the endogenous variations of ERK activity, and to test for possible entrainment of ERK oscillations by optogenetic stimulation. The interval of 30 min between two stimuli allows for the return of nuclear ERK activity to its prestimulation level.

The optogenetic stimulation was carried out in sets of seven light doses, and each set was repeated 20 times. The light doses are changed by modulating the illumination time in increasing order: 200, 300, 500, 700, 1000, 1500, and 2000 ms, while the laser power was kept constant at about 200 μW in order to diminish the effects of nonlinear laser power output. Previously, a wide range of light doses was applied to obtain dose-response curves throughout several experiments with many cells to identify the maximal sensitivity range of an average cell, and the chosen light doses were chosen to fall within this range. Given the duration of the cell cycle, cell migration, and other effects that set a limit on the number of stimulations that can be applied on a single cell, the pattern of stimulation with a repeating set of increasing light doses was chosen over a randomized one to maximize the chances of obtaining the highest number of repeats per light dose.

4. Data analysis

The image segmentation and tracking of the nuclei in the H2B channel were carried out in iLastik software (version 1.4.0). Next, the segmented nuclei were used to extract the average nuclear ERK reporter signal from the images in the ERK-KTR channel. Equally, the average ERK reporter signal contained in a thin ring around the nucleus was extracted for the subsequent calculation of the cytosolic-to-nuclear ratio of the reporter. A ring thickness of 4 px provides the most robust readout and the best tradeoff between acquiring enough cytoplasmic signal and remaining within the boundaries of the cell in cases of the nucleus being in close proximity to the membrane. Using a custom-written Matlab data analysis pipeline, the nucleus-tracking trajectories were matched with the ERK signal readout, assigning each cell a unique ID. The movement of the cells or fluorescent debris passing over the field of view causes occasional issues in segmentation and tracking, resulting in missing frames—i.e., no information on the ERK activity. To ensure data quality, only the cells with an ERK signal in 95% of the total number of frames are selected for the next step of the analysis. This criterion automatically excludes cells that underwent mitosis, migration in or out of the field of view during the acquisition, and cells with significant morphological changes, the latter of which could indicate aberrant cell physiology. The magnitude of nuclear ERK activity is quantified as the ratio between the cytosolic and the nuclear ERK signal described above. To calculate the dose-response curves, single-cell ERK time trajectories were detrended using a moving averaging window of 100 frames before being divided into intervals of 15 frames, starting with the timepoint of the stimulation. The raw and detrended trajectories, as well as the impact of different detrending methods on the estimation of mutual information, are presented in Figs. S18 and S19 of the SM [24]. The first two principal components obtained by principal component analysis of the ensemble of response trajctories are depicted in Fig. S20 of the SM [24]. The light doses are calculated as the integral of the light power measured with the power meter over the time interval of stimulation.

5. Numerical simulations

Numerical simulations of optogenetic MAPK pathway activation were carried out by implementing the kinetic model

from [25] in matlab. The activation of ERK is read out as the ratio between the cytosolic and nuclear KTR, analogously to the experiments. The parameters—reaction rates and initial concentrations—were determined from experimental data [25] and inferred using the Nested Sampling algorithm described in [41], kindly provided by the authors. The virtual cells were created by generating 400 sets of parameters with up to 18% randomly applied Gaussian white noise. To mimic the experimental variability in the light dose, up to 10% Gaussian white noise was applied to the light input parameter. The light doses used in the simulations were chosen to yield activation trajectories and dose-response curves that closely resemble experimental ones (Fig. S8 of the SM [24]). Additionally, a saturation threshold for activation was determined based on the experiments. Each of the 400 virtual cells were stimulated with the seven light doses, spaced in time to allow KTR to return to its initial value, repeating this process 1000 times.

[1] S. J. Gershman, P. E. Balbi, C. R. Gallistel, and J. Gunawardena, Reconsidering the evidence for learning in single cells, Elife **10**, e61907 (2021).

[2] T. J. Perkins and P. S. Swain, Strategies for cellular decision-making, Mol. Syst. Biol. **5**, 326 (2009).

[3] C. Y. F. Huang and J. E. Ferrell, Ultrasensitivity in the mitogen-activated protein kinase cascade, Proc. Natl. Acad. Sci. USA **93**, 10078 (1996).

[4] A. Ram, D. Murphy, N. DeCuzzi, M. Patankar, J. Hu, M. Pargett, and J. G. Albeck, A guide to ERK dynamics, Part 1: Mechanisms and models, Biochem. J. **148**, 887 (2023).

[5] A. Ram, D. Murphy, N. DeCuzzi, M. Patankar, J. Hu, M. Pargett, and J. G. Albeck, A guide to ERK dynamics, Part 2: Downstream decoding, Biochem. J. **480**, 1909 (2023).

[6] G. D. Potter, T. A. Byrd, A. Mugler, and B. Sun, Dynamic sampling and information encoding in biochemical networks, Biophys. J. **112**, 795 (2017).

[7] F. Grabowski, P. Czyż, M. Kochańczyk, and T. Lipniacki, Limits to the rate of information transmission through the MAPK pathway, J. R. Soc. Interface **16**, 20180792 (2019).

[8] R. Cheong, A. Rhee, C. J. Wang, I. Nemenman, and A. Levchenko, Information transduction capacity of noisy biochemical signaling networks, Science **334**, 354 (2011).

[9] A. Vazquez-Jimenez and J. Rodriguez-Gonzalez, On information extraction and decoding mechanisms improved by noisy amplification in signaling pathways, Sci. Rep. **9**, 14365 (2019).

[10] W. Bialek, *Biophysics: Searching for Principles* (Princeton University Press, Princeton, NJ, 2012).

[11] M. Bauer, M. D. Petkova, T. Gregor, E. F. Wieschaus, and W. Bialek, Trading bits in the readout from a genetic network, Proc. Natl. Acad. Sci. USA **118**, e2109011118 (2021).

[12] J. Selimkhanov, B. Taylor, J. Yao, A. Pilko, J. Albeck, A. Hoffmann, L. Tsimring, and R. Wollman, Accurate information transmission through dynamic biochemical signaling networks, Science **346**, 1370 (2014).

[13] B. A. Kramer, J. S. del Castillo, and L. Pelkmans, Multimodal perception links cellular state to decision-making in single cells, Science **377**, 642 (2022).

[14] R. Suderman and E. J. Deeds, Intrinsic limits of information transmission in biochemical signaling motifs, Interface Focus **8**, 20180039 (2018).

[15] M. B. Elowitz, A. J. Levine, E. D. Siggia, and P. S. Swain, Stochastic gene expression in a single cell, Science **297**, 1183 (2002).

[16] A. Levchenko and I. Nemenman, Cellular noise and information transmission, Curr. Opin. Biotechnol. **28**, 156 (2014).

[17] S. Mitchell and A. Hoffmann, Identifying noise sources governing cell-to-cell variability, Curr. Opin. Syst. Biol. **8**, 39 (2018).

[18] S. Tay, J. J. Hughey, T. K. Lee, T. Lipniacki, S. R. Quake, and M. W. Covert, Single-cell NF-κB dynamics reveal digital activation and analog information processing, Nature (London) **466**, 267 (2010).

[19] M. A. Vis, K. Ito, and S. Hofmann, Impact of culture medium on cellular interactions in in vitro co-culture systems, Front. Bioeng. Biotechnol. **8**, 911 (2020).

[20] A. Goetz, H. Akl, and P. Dixit, The ability to sense the environment is heterogeneously distributed in cell populations, Elife **12**, RP87747 (2024).

[21] J. E. Toettcher, O. D. Weiner, and W. A. Lim, Using optogenetics to interrogate the dynamic control of signal transmission by the Ras/Erk module, Cell **155**, 1422 (2014).

[22] T. Jetka, K. Nienałtowski, T. Winarski, S. Błoński, and M. Komorowski, Information-theoretic analysis of multivariate single-cell signaling responses, PLoS Comput. Biol. **15**, e1007132 (2019).

[23] N. Kim, J. M. Kim, M. Lee, C. Y. Kim, K. Y. Chang, and W. D. Heo, Spatiotemporal control of fibroblast growth factor receptor signals by blue light, Chem. Biol. **21**, 903 (2014).

[24] See Supplemental Material at http://link.aps.org/supplemental/10.1103/pyf8-y4kt for additional figures concerning the experimental variability, numerical simulations, data processing, and raw imaging timeseries.

[25] C. Dessauges, J. Mikelson, M. Dobrzyński, M. Jacques, A. Frismantiene, P. A. Gagliardi, M. Khammash, and O. Pertz, Optogenetic actuator–ERK biosensor circuits identify MAPK network nodes that shape ERK dynamics, Mol. Syst. Biol. **18**, e10670 (2022).

[26] C. de la Cova, R. Townley, S. Regot, and I. Greenwald, A real-time biosensor for ERK activity reveals signaling dynamics during *C. Elegans* cell fate specification, Dev. Cell **42**, 542 (2017).

[27] K. Aoki, Y. Kumagai, A. Sakurai, N. Komatsu, Y. Fujita, C. Shionyu, and M. Matsuda, Stochastic ERK activation induced by noise and cell-to-cell propagation regulates cell density-dependent proliferation, Mol. Cell **52**, 529 (2013).

[28] J. Ish-Horowicz and J. Reid, Mutual information estimation for transcriptional regulatory network inference, bioRxiv (2017), https://doi.org/10.1101/132647.

[29] D. G. Hernández and I. Samengo, Inferring a property of a large system from a small number of samples, Entropy **24**, 125 (2022).

[30] M. Z. Wilson, P. T. Ravindran, W. A. Lim, and J. E. Toettcher, Tracing information flow from ERK to target gene induction reveals mechanisms of dynamic and combinatorial control, Mol. Cell **67**, 757 (2017).

[31] G. Tkačik, C. G. Callan, and W. Bialek, Information flow and optimization in transcriptional regulation, Proc. Natl. Acad. Sci. USA **105**, 12265 (2008).

[32] D. Ellison, A. Mugler, M. D. Brennan, S. H. Lee, R. J. Huebner, E. R. Shamir, L. A. Woo, J. Kim, P. Amar, I. Nemenman, A. J. Ewald, and A. Levchenko, Cell-cell communication enhances the capacity of cell ensembles to sense shallow gradients during morphogenesis, Proc. Natl. Acad. Sci. USA **113**, E679 (2016).

[33] A. Stanoev, A. P. Nandan, and A. Koseska, Organization at criticality enables processing of time-varying signals by receptor networks, Mol. Syst. Biol. **16**, e8870 (2020).

[34] T. J. Aikin, A. F. Peterson, M. J. Pokrass, H. R. Clark, and S. Regot, MAPK activity dynamics regulate non-cell autonomous effects of oncogene expression, Elife **9**, e60541 (2020).

[35] P. A. Gagliardi, M. Dobrzyński, M. A. Jacques, C. Dessauges, P. Ender, Y. Blum, R. M. Hughes, A. R. Cohen, and O. Pertz, Collective ERK/AKT activity waves orchestrate epithelial homeostasis by driving apoptosis-induced survival, Dev. Cell **56**, 1712 (2021).

[36] P. Ender, P. A. Gagliardi, M. Dobrzyński, A. Frismantiene, C. Dessauges, T. Höhener, M. A. Jacques, A. R. Cohen, and O. Pertz, Spatiotemporal control of ERK pulse frequency coordinates fate decisions during mammary acinar morphogenesis, Dev. Cell **57**, 2153 (2022).

[37] M. Kramar, L. Hahn, A. M. Walczak, T. Mora, and M. Coppey, Data for "Single cells can resolve graded stimuli," BioStudies (2025), https://www.ebi.ac.uk/biostudies/bioimages/studies/S-BIAD2275.

[38] A. Kraskov, H. Stögbauer, and P. Grassberger, Estimating mutual information, Phys. Rev. E **69**, 066138 (2004).

[39] Y. Tang, A. Adelaja, F. X. Ye, E. Deeds, R. Wollman, and A. Hoffmann, Quantifying information accumulation encoded in the dynamics of biochemical signaling, Nat. Commun. **12**, 1272 (2021).

[40] L. Hahn, A. M. Walczak, and T. Mora, Dynamical information synergy in biochemical signaling networks, Phys. Rev. Lett. **131**, 128401 (2023).

[41] J. Mikelson and M. Khammash, Likelihood-free nested sampling for parameter inference of biochemical reaction networks, PLoS Comput. Biol. **16**, e1008264 (2020).